Biosensors and Bioelectronics 201 (2022) 113919

Contents lists available at ScienceDirect

Biosensors and Bioelectronics

journal homepage: www.elsevier.com/locate/bios

Smartphone integrated handheld Long Range Surface Plasmon Resonance based fiber-optic biosensor with tunable SiO_2 sensing matrix

Surbhi Jain [a], Ayushi Paliwal [b], Vinay Gupta [a,1], Monika Tomar [c,*]

[a] Department of Physics and Astrophysics, University of Delhi, Delhi, 110007, India
[b] Department of Physics, Deshbandhu College, University of Delhi, Delhi, 110007, India
[c] Department of Physics, Miranda House, University of Delhi, Delhi, 110007, India

ARTICLE INFO

Keywords:
Smartphone
Optical fiber
LRSPR
SiO_2
Tunable refractive index

ABSTRACT

In the present work, a novel smartphone assisted fiber optic (FO)-Long range surface plasmon resonance (LRSPR) based biosensor is proposed. In the developed biosensor, the inbuilt color sensitive property of the digital camera present in the smartphone is used for the monitoring of blue and red color channel intensities. This will replace the most exploited diffraction gratings or narrow band filters used for analyzing the spectral data in reported smartphone based SPR sensors. The proposed technique helps in improving the sensitivity and reduces the chances of wrong detection. For the first time, SiO_2 nanostructured film is employed as the dielectric sensing layer to excite the Long range surface plasmons (LRSPs) in the dielectric-metal-dielectric configuration. The proposed FO-LRSPR biosensor possess limit of detection of 0.02 mM and sensitivity of 0.9/mM and, for uric acid detection in the 0.1 mM–1 mM concentration range. The novel fabricated sensor which is found to be stable up to 24 weeks can be effectively utilized in health sector and environment monitoring and it possess the ability of point-of-care detection, even in rural and remote areas.

1. Introduction

The ever-growing demand for modernization has pushed people to look out for time saving and efficient techniques, which can be utilized in day-to-day activities. In modern times, need for point of care devices (POCDs) has grown tremendously owing to the increasing pace of life. POCDs provide many advantages over the conventional lab based sensing devices such as on site detection, early diagnosis etc. In remote locations, due to lack of conventional analytical tools, such rapid on-site detection techniques are essentially required and pursued for early diagnosis and environmental monitoring. Moreover, the conventional lab based testing analysis needs trained professionals, high-end instruments, complicated procedures and expensive lab tests. These processes are definitely highly sensitive, accurate and provide advanced modern diagnostics, which is quite beneficial for developed countries. However, for developing nations with limited resources, these methods are not appropriate for on-site investigations as they consume more time and are not economical.

Numerous electrical/optical techniques, for e.g. colorimetric immunoassays and paper-based devices to detect HIV, addressing the problems faced in the field of POCDs and on field detection have been proposed in the past many years (Potyrailoet al., 2012), (Rakow and Suslick, 2000). These techniques inspite of having the advantage of naked eye detection requires data processing, image capturing and complex amplification process for enhancing the sensitivity and precision.

A significant improvement in healthcare services requires the communization of these services to better quality and inferior cost. Some concerns like patient comfort, early diagnosis, close monitoring are the main objectives that healthcare providers are struggling to achieve. For the last two decades, a significant development in the lab-on-chip platforms has introduced many novel techniques for quick detection of prevalent diseases. Devices based on such techniques are possessed with certain critical assets like short turn-around-time, portability, connectivity and cost-effective. The progressions in the fabrication of such lab on chip devices have enabled the point of care testing in not only the areas with limited resources but also facilitated at-home monitoring of senior citizens in developed countries as well. The main blockage into the commercialization of such lab on chip based POCDs is the need of miniaturization and combining various components on a single chip.

* Corresponding author.
E-mail address: monikatomar@gmail.com (M. Tomar).
[1] The author passed away prior to the submission of this paper. This is one of the last works of him.

https://doi.org/10.1016/j.bios.2021.113919
Received 2 July 2021; Received in revised form 14 October 2021; Accepted 22 December 2021
Available online 29 December 2021

Amongst the existing POCDs, mobile phones is a popular choice because of their rapidly advancing functions, global ubiquity, capability to directly couple with optical methods such as fluorescence, chemiluminescence, transmittance/absorbance, guided waves spectroscopy, and Surface Plasmon Resonance (SPR) (Tsenget al., 2010)–(Zangheriet al., 2015). Mobile phones have become an essential part of a common person's daily life. Due to their easy availability and reasonable prices, mobile phones have found great deal of use in healthcare sector. The integration of mobile phones with lab on chip devices has emerged as a revolution in the field of diagnostic devices and integrated screening. Mobile phones are equipped with sensitive cameras having high pixel count, integrated light sources, touchscreen displays, powerful CPUs and advanced connectivity features, which make them a ubiquitous device. This holds a solid foundation for the recent development in the field of smart phone assisted optical detection techniques. There are a number of biosensing techniques like colorimetric detection, flow cytometry, immunodiagnostic assays and surface plasmon resonance (SPR), which have utilized smartphone for the sensing purposes. Smartphone biosensors based optical and electrical detection methods are discussed in details elsewhere (Roda et al., 2016).

In conventional immunoassays like Enzyme-linked immunosorbent assay (ELISA), labeling of antibodies needs to be done to acquire a detectable signal and the washing procedure is also tedious, which make them a difficult choice for on-site applications. Surface plasmon resonance (SPR) is widely utilized in the biosensing field for environmental monitoring, food safety, clinical analysis and disease diagnosis owing to its numerous advantageous properties such as low-cost, label-free, and high sensitivity. An intensive development has been observed in the SPR-based sensors over the past two decades. However, the bottleneck in the commercialization of SPR biosensors lies in its low sensitivity when the analyte under study has a size similar to or bigger than the wavelength of the incident light. Moreover, miniaturization and high throughput of the setup used in the SPR based biosensing is another challenge encountered by researchers (Mudanyali et al., 2012), (Burgess and Eastman, 2006).

These limitations can be overcome by a relatively new optical technique called Long Range Surface Plasmon Resonance (LRSPR), which are extensively explored by the researchers in the past few years (Berini, 2009)– (Paliwal et al., 2018). Excitation of Long Range Surface Plasmons (LRSPs) in the symmetric dielectric-metal-dielectric structure causes the formation of highly sensitive Long Range Surface Plasmon wave, which can accurately detect any change in the dielectric properties of its environment. LRSPR based sensors are known to possess higher sensitivity as compared to conventional SPR based sensors (Méjard et al., 2014), (Wark et al., 2005). Moreover, optical fiber has been an active choice over the prism coupled arrangement in the fabrication of SPR based sensors owing to advantages such as miniaturization, remote sensing, flexibility and online monitoring (Gupta and Verma, 2009). There has been a very limited research on optical fiber based LRSPR sensors. Cytop and Teflon are the polymers mainly used in the excitation of LRSPs. However, they suffer from certain disadvantages like low quality thin films, degradation at elevate temperatures and unstable under harsh environmental conditions. In our previous work, it is shown that the refractive index of nanostructured SiO_2 can be tailored (Jain et al., 2020a). It is reported that the matching between the two dielectrics (SiO_2 and the analyte) is a crucial factor for the excitation of LRSPs (Berini, 2009). Hence, use of an appropriate deposition technique and parameters are essentially required to obtain the SiO_2 thin film having refractive index ~ 1.33 (refractive index of water). Plasma Enhanced Chemical Vapor Deposition (PECVD) is considered as the most appropriate technique due to the ability of coating uniform optical quality thin film. In the present work, a fiber-optic based LRSPR biosensor has been reported using SiO_2 as the dielectric layer with refractive index ~ 1.33. As a model analyte, uric acid is chosen. Well being of an individual requires the appropriate maintaining of uric acid levels in a human body. In a healthy human body, the physiological range of uric acid is from 0.16 mM to 0.43 mM (Arora et al., 2014). To the best of our knowledge, no fiber-optic LRSPR based uric acid has been reported till date. However a few uric acid biosensors based on SPR are proposed in literature. Kant et al. proposed a fiber-optic SPR sensor with Si sensing layer for detection of uric acid in the 0.1 mM–0.9 mM concentration range. They reported a LOD of 0.032 mM (Kant et al., 2016a). Sarikaya et al. utilized prism coupling arrangement in Kretschmann configuration to fabricate molecular imprinted SPR sensor for uric acid detection in 2.97 μM to 0.24 mM concentration range (Göçenoğlu Sarıkaya et al., 2017). They used embossed poly (HEMA-MAC)-Fe3+ nanoparticles as the sensing layer. However, the preparation of sensor is a complex and tedious process (Göçenoğlu Sarıkaya et al., 2017). Batumalay et al. reported uric acid sensors with three different sensing layers: ZnO coated tapered optical fiber, Graphene and single wall CNT (SWCNT) polyethylene oxide composite (Batumalay et al., 2014a)–(Batumalay et al., 2014b). The LOD achieved by the sensors 0.03 mM, 0.045 mM and 0.04 mM respectively (Batumalay et al., 2014a)–(Batumalay et al., 2014b). However no selectivity studies were performed. To effectively overcome these bottlenecks, in the present work fiber optic-LRSPR sensor is used for uric acid detection in the 0.1 mM – 1 mm concentration range which is further integrated with a smartphone to make it portable, handheld and economical. To the best of our knowledge, this paper presents the first ever Fiber optic-LRSPR based smartphone assisted biosensor.

2. Experimental section

2.1. Growth of SiO_2 thin film utilizing PECVD technique

SiO_2 nanostructured thin films on Si substrate are prepared utilizing PECVD method under varying deposition pressure from 500 mTorr to 650 mTorr, keeping the thickness constant at 200 nm. The deposition conditions of nanostructured SiO_2 films are listed in the Supplementary Table S1.

2.2. Characterization studies

Fourier Transform Infrared (FTIR) spectroscopy, Atomic force microscopy (AFM), and Energy dispersive x-ray (EDAX) analysis were performed on the deposited SiO_2 nanostructured thin films to study their morphological and structural studies, whose details are discussed in the supplementary file. Further, ellipsometry and SPR studies were carried out to determine the refractive index of the deposited nanostructured SiO_2 thin films.

3. Results and discussions

3.1. Refractive index optimization using SPR and ellipsometry

Refractive index values of the deposited nanostructured SiO_2 thin films were determined by SPR studies. Fig. 1 depicts the reflectance curves obtained for the prism/air-gap/Au/SiO_2/Si system for the SiO_2 films deposited at different growth pressures. In Fig. 1, symbols represent the experimental data points and the solid black line represents the corresponding theoretical fitted curves. All the SPR measurements were taken in the Otto configuration, whose details are described in our earlier work (Jain et al., 2020b). The inset of the Figure represents the SPR reflectance curve attained for the prism/air-gap/Au/Si configuration. It could be inferred from the inset of Fig. 1, that the resonance angle (θspr) i.e. the angle at which minimum reflectance (R_{min}) is observed is shifting towards the higher side when the dielectric medium changes from Au/Si to Au/SiO_2/Si. This change is due to the variation in refractive index value of dielectric medium in the ambient of Au (metal) thin film. Now, for the SiO_2 nanostructured thin films grown at different deposition pressure, the corresponding SPR reflectance curves show diverse values of θ_{spr} and R_{min}. This is accredited to the change in the

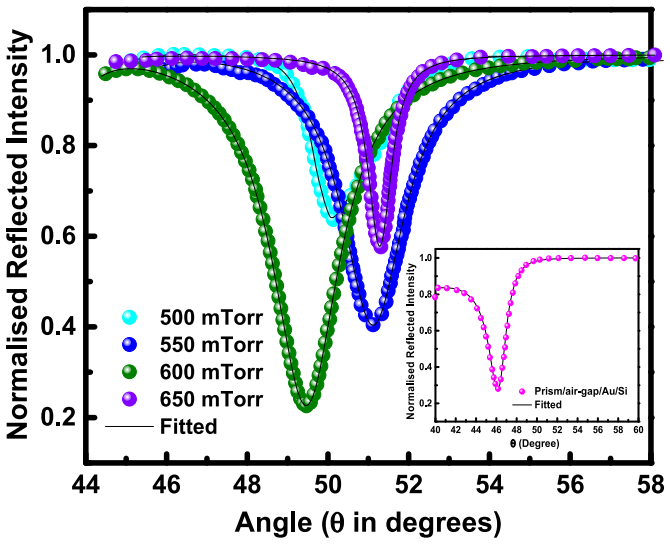

Fig. 1. SPR reflectance curves of Prism/air-gap/Au/SiO_2/Si configuration for SiO_2 films fabricated at increasing deposition pressure (Inset: SPR reflectance curve of prism/air-gap/Au/Si configuration).

optical property (refractive index) of the deposited SiO_2 nanostructured films as the deposition pressure is varied. Further, the refractive index values of the fabricated nanostructured SiO_2 films at different growth pressure is determined using Fresnel's equations (Dewan et al., 2018) and are shown in Supplementary Table S2. The value of refractive index corresponding to the fabricated SiO_2 nanostructured films are lower as compared to that of the bulk SiO_2 (1.49). The SiO_2 film grown at 600 mTorr pressure is found to have the refractive index value ~ 1.33 (Supplementary Table S2).

The obtained refractive index results with SPR were verified with Ellipsometry and it was found that they are in close proximity of each other. Now, the SiO_2 nanostructured thin film having thickness 200 nm and deposition pressure of 600 mTorr is used in the development of FO-LRSPR biosensor.

3.2. Bio-sensing characteristics

To fabricate the FO-LRSPR biosensor, the multimode silica clad silica core optical fiber with 0.37 numerical aperture (NA) and core diameter of 400 μm is used. A surgical blade is used to cleave out 1 cm length of the cladding portion from the optical fiber of 10 cm length. The fiber with the cleaved-clad is meticulously washed with Isopropyl Alcohol, Acetone and Trichloroethylene sequentially. Subsequently cleaning in indigenously developed plasma cleaner was done to get rid of any residual organic impurity. Further, the optimized SiO_2 nanostructured film having refractive index ~ 1.33 is deposited using PECVD technique on cleaved portion of the optical fiber, as the first dielectric layer. On top of that, Au thin film having optimized thickness of 20 nm is deposited by thermal evaporation technique. Uricase enzyme of 1 mM concentration is immobilized on the top of Au layer using physical adsorption technique. The schematic of the prepared sensor configuration uricase/Au/SiO_2/optical-fiber structure is given in Fig. 2(a). The digital photograph of the 1 cm length of the cleaved clad portion is shown below in Fig. 2 (b). An appreciable color contrast can be seen between the two portions: 1 cm portion from where the cladding is removed and the rest of the portion with cladding intact. We also analyzed the cross sectional view of the proposed fiber optic-LRSPR sensing structure (uricase/Au/SiO_2/core) shown in Fig. 2 (a) using SEM analysis. Fig. 2 (c) presents the cross sectional view of the optical fiber. Since the size of the enzyme (Uricase) immobilized on the Au/SiO_2/core structure is quite large (a few microns), we could not see the individual layers of SiO_2 (~200 nm) and Au (~ 20 nm) deposited consecutively on the cleaved clad portion i.e. on core of the optical fiber. Hence, to justify the binding of Uricase enzyme on the Au/SiO_2/core structure, we performed SEM analysis on the top portion of the optical fiber, which is shown in Fig. 2 (d). It can be verified from Fig. 2 (d) that uricase enzyme is successfully adsorbed on the Au/SiO_2/core structure (globular structures can be seen on the surface) and can be effectively utilized to provide binding sites for uric acid. Further, a glass flow cell is built in-house to keep uric acid in contact with the fabricated uricase/Au/SiO_2/optical-fiber structure. Finally, the required LRSPR structure i.e. uric acid-uricase/Au/SiO_2/optical-fiber is built in which uric acid-uricase and SiO_2 act as the two dielectrics having identical refractive index in the standard LRSPR dielectric-metal-dielectric structure. Schematic of the prepared sensor structure is given in Fig. 2(e).

3.3. Avantes spectrometer based sensing

To check the feasibility of the prepared LRSPR biosensor structure, uric acid sensing is performed using a Halogen lamp (Make: Avantes) and a spectrometer (Make: Avantes). The schematic of the same is given in Fig. 2(e). A halogen lamp is used to incident light inside the optical fiber such that total internal reflection occurs and an evanescent wave is generated which interacts with the LRSPs formed as a result of the constructive interference occurring amongst the Surface plasmon waves originated at the two identical metal-dielectric interfaces (uric acid-uricase/Au and Au/SiO_2). The transmitted light from another optical fiber end is captured by the spectrometer as shown in Fig. 2(e). The entire structure of the sensor is positioned on an optical stand having the capability of x-y adjustments. Firstly, for reference, Phosphate Buffer Saline (PBS) solution having PH value of 7 is flown through the glass flow cell and the corresponding LRSPR transmittance curve is recorded. The LRSPR transmittance curves were recorded for different concentrations of uric acid (0.01–1 mM) flown one by one through the glass flow cell. The glass flow cell was washed with buffer solution after each measurement, as a result the transmittance curve is traced back to its initial position (the one obtained with only PBS solution) and after that subsequent concentration of uric acid is introduced. The wavelength at which lowest transmittance is observed is termed as Resonance wavelength (λ_{LRSPR}). The obtained LRSPR biosensing characteristic transmittance curves are shown in Fig. 3(a). As observed from Fig. 3(a), the transmittance curve shifts towards the right side as the concentration of uric acid is increased, which is attributed to the variation in the second dielectric medium (uric acid-uricase) as the concentration of uric acid is varied.

3.4. Sensing mechanism

The normalized transmitted power, P_{trans}, for a fiber optic LRSPR sensor is (Gupta and Verma, 2009):

$$P_{trans} = \frac{\int_{\theta_{cr}}^{\frac{\pi}{2}} \frac{R_p^{N_{ref}(\theta)} n_1^2 \sin\theta\cos\theta}{\left(1-n_1^2\cos^2\theta\right)^2} d\theta}{\int_{\theta_{cr}}^{\pi/2} \frac{n_1^2 \sin\theta\cos\theta}{\left(1-n_1^2\cos^2\theta\right)^2} d\theta}. \quad (1)$$

where, R_p is the reflectance for the ray with polarization normal to the core-cladding interface and is defined as the reflectance for the four layered system (Uric acid-Uricase/Au/SiO_2/core) at an incident angle θ given by (Paliwal et al., 2018):

$$R_{1234} = \left| \frac{r_{12} + r_{234} * f_2}{1 + r_{12} * r_{234} * f_2} \right|^2 \quad (2)$$

$$r_{234} = (r_{23} + r_{34} * f_3) / (1 + r_{23} * r_{34} * f_3) \quad (3)$$

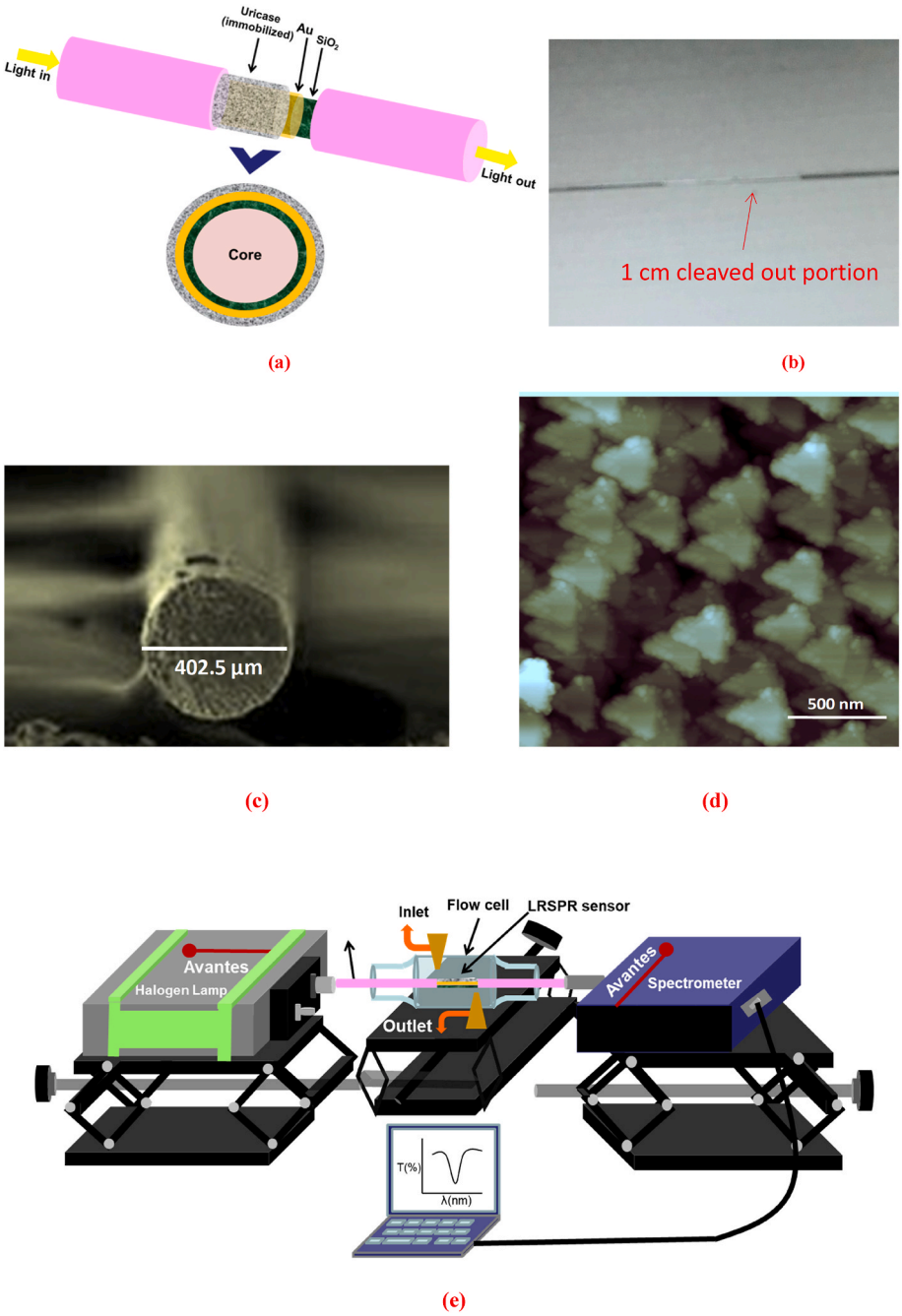

Fig. 2. Schematic of the proposed (a) uricase/Au/SiO_2/optical fiber sensor structure, (b) Enlarged digital photograph of 1 cm length of the cleaved clad portion (c) Cross-sectional and, (d) Top view, SEM image of the uricase/Au/SiO_2/core LRSPR sensing structure, (e) FO-LRSPR biosensing setup using Avantes spectrometer for sensing uric acid.

$$r_{ik} = \frac{\left(\frac{k_{zi}}{\varepsilon_i} - \frac{k_{zk}}{\varepsilon_k}\right)}{\left(\frac{k_{zi}}{\varepsilon_i} + \frac{k_{zk}}{\varepsilon_k}\right)} \tag{4}$$

$$k_{zi} = \frac{2\pi}{\lambda}\left(\varepsilon_i - \varepsilon_1 \sin^2\theta\right)^{\frac{1}{2}} \tag{5}$$

$$f_i = \exp(s_2 * (0 + 1j)) \tag{6}$$

$$s_i = 2 * k_{zi} * d_i \tag{7}$$

where, ε_i with $i = 1$ to 4 are the dielectric constants of uric acid-uricase, Au, SiO_2 and core respectively, λ is wavelength of the incident light, and θ is incident angle of the light. The d_1, d_2 and d_3 are thickness of the semi-infinite dielectric media (uric acid-uricase), Au and SiO_2 layer respectively.

$N_{ref}(\theta)$ represents the number of reflections incurred by a ray making an angle θ with the normal to the core-SiO_2 layer interface in the sensing region, while the critical angle of the core-SiO_2 interface for a given optical fiber is given by:

$$\theta_{cr} = \sin^{-1}\left(\frac{n_{SiO_2}}{n_1}\right) \tag{8}$$

where, n_{SiO_2} is the refractive index of the SiO_2 layer and n_1 is the refractive index of the core of the optical fiber,

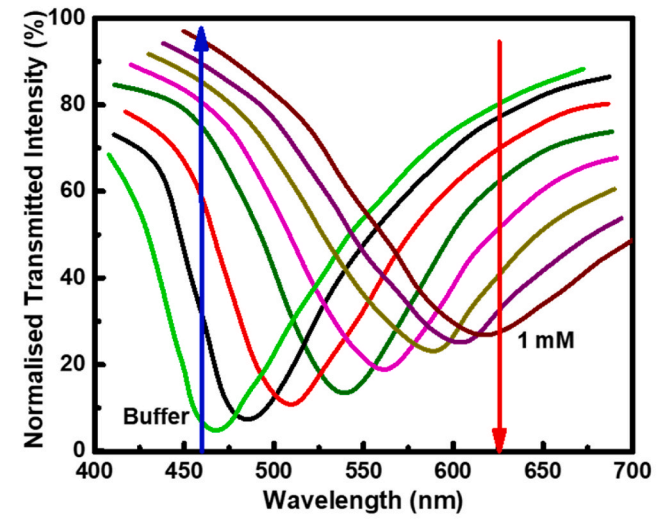

(a)

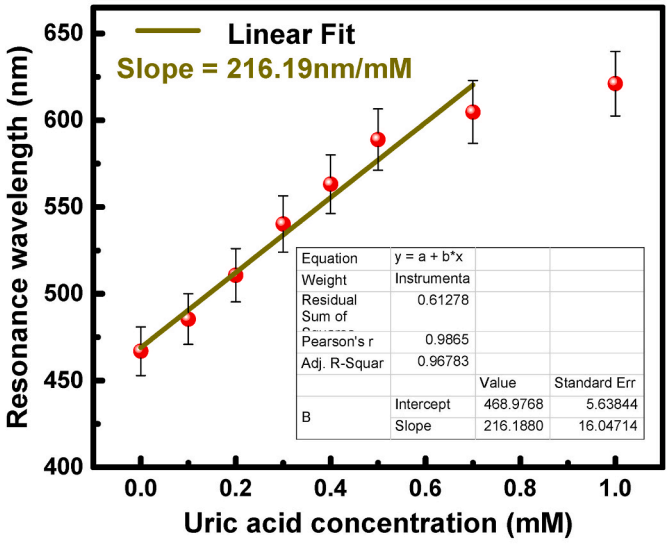

(b)

Fig. 3. LRSPR transmission curves for the increasing uric acid concentration, (b) Resonance wavelength change with the increasing uric acid concentration.

$$N_{ref}(\theta) = \frac{L}{2\rho \tan\theta} \tag{9}$$

L and ρ represent the length of the exposed sensing region and the fiber core radius, respectively. The output transmitted power, P_{tans}, is calculated from eq. (1) for the case of excitation of long surface plasmons using on-axis light launching in the fiber.

Now, as we change the uric acid concentration, the reflectance value in equation (2) correspondingly changes as a result of refractive index variation in the dielectric media (uric acid-uricase) of the uric acid-–uricase/Au/SiO_2/core sensor structure. This leads to a change in the transmittance power in equation (1). The electromagnetic field allied to the LRSPs is strongly dependent on the refractive index of the second dielectric, therefore as the concentration of uric acid is increased, the propagation constant of the LRSP wave changes. This accounts for the change in resonance conditions of the excited LRSPs and as a result of which, the resonance wavelength is shifted (Fig. 3(a)). The change in concentration of uric acid leads to the change in the refractive index of the second dielectric (uric acid-uricase) in the uric acid-uricase/Au/SiO_2/optical-fiber sensor structure. When uricase (enzyme) catalyses the reaction of uric acid (analyte) with oxygen, following chemical reaction takes place (Kant et al., 2016b):

$$\text{Uric acid} + O_2 + H_2O \Leftrightarrow^{uricase} \text{Allantoin} + CO_2 + H_2O_2$$

As can be observed from Fig. 3 (a), a blue shift is observed in the resonance wavelength as the uric acid concentration is increased. Allantoin and H_2O_2 are products of the biochemical reaction taking place between uric acid and uricase. As we increase the uric acid concentration in PBS, concentration of Allantoin and H_2O_2 also increases. Since refractive index of Allantoin (1.615) ('s-Gravenmade et al., 2010) is less than the refractive index of uric acid (1.721) (Ringertz, 1965), a continuous decrease in the refractive index of the bulk sensing media takes place as the concentration of uric acid is increased. Since wavelength has inverse dependency on refractive index, it is expected for the wavelength to shift towards higher side as the refractive index is decreased.

A calibration curve showing the change in resonance wavelength with respect to the concentration of uric acid is presented in Fig. 3 (b). Good linearity is observed for the 0.01–0.7 mM concentration range of uric acid. This proves that the fabricated FO-LRSPR biosensor possess linear response much beyond the physiological range of uric acid (0.16 mM–0.43 mM) in a healthy human body (Jindal et al., 2017). As we increase the concentration of uric acid from 0.01 mM to 0.7 mM, λ_{LRSPR} value increases linearly from 485 nm to 605 nm (Fig. 3 (b)). The sensing response saturates when the uric acid concentration is increased beyond 0.7 mM. This trend is similar to what has been observed in the reported sensors for higher concentration of uric acid (Wark et al., 2005), (Luet al., 2012). The standard deviation was found out to be less than 5%, when for uric acid concentration, the measurement was repeated for 5 times. The prepared FO-LRSPR biosensor has a high sensitivity of 216.19 nm/mM towards the detection of uric acid, as anticipated from the slope of calibration curve (Fig. 3 (b)). The detection limit (LOD) of the proposed sensor is estimated as 0.05 mM (Srivastava et al., 2011).

3.5. Smartphone based sensing

The complementary metal oxide semiconductor (CMOS) digital cameras installed in the smartphones and white light LED have been used, as detector and the light source respectively, for the fabrication of dual-color fiber optic LRSPR sensor. The digital camera of a smartphone has inbuilt color filters having red-green-blue (RGB) passbands which can be utilized for measuring the light intensity corresponding to different color channels. A software application capable of analyzing colored image (Name: Color Analysis) is used for determining the red and blue channels intensity from the captured image, in real time.

The schematic for the fabricated smartphone integrated FO-LRSPR sensor setup is depicted in Fig. 4 (a). One end of the optical fiber is coupled to the white LED from where the light is launched into the fiber. Other end is coupled with camera of the smartphone, where the transmitted light is captured in the form of an image with a resolution of 1080 × 2340. For the evaluation of the fabricated sensor, the cleaved-clad sensing portion (uricase/Au/SiO_2/optical fiber) is held in contact with the analyte (uric acid) with the help of a circular container (Fig. 4 (a)). One by one, different concentrations of uric acid ranging from 0.05 to 1 mM are filled and the consequent transmitted light is acquired. The fiber optic sensor is properly washed in PBS buffer after each measurement. All the experiments were performed in a dark room at room temperature. The normalized intensity determined for the red and blue channel corresponding to different concentrations of uric acid is shown in Fig. 4 (b). It can be inferred from Fig. 4 (b), that the intensity of blue color channel increases and that of red color channel decreases with increase in the uric acid concentration. As observed in Fig. 3 (a), the resonance wavelength is shifted towards higher wavelength with the increase in the uric acid concentration i.e. blue shift in the wavelength is

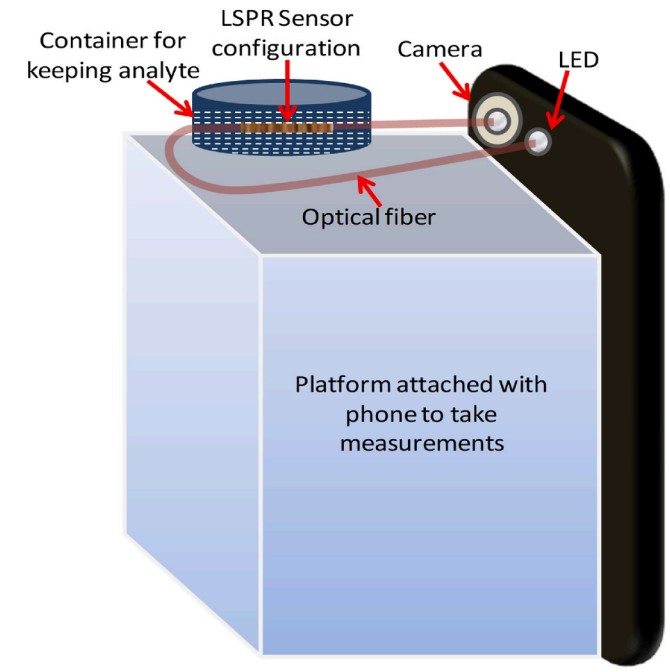

(a)

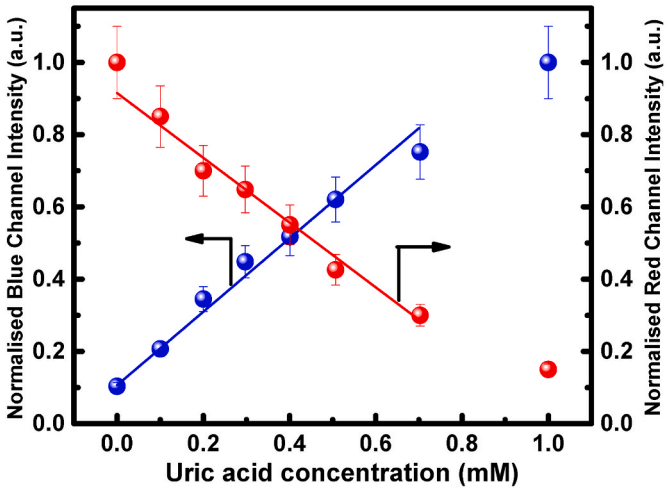

(b)

Fig. 4. (a) Schematic of the prepared smartphone assisted FO-LRSPR uric acid biosensor, (b) Normalized blue and red color intensity with increasing concentration of uric acid. (For interpretation of the references to color in this figure legend, the reader is referred to the Web version of this article.)

observed. This trend is in harmony with the observed increased in the intensity of blue color channel. Also it can be seen from Fig. 3 (a) that near the resonance dip, intensity at lower wavelength side (blue color region) increases and at the higher wavelength side (red color region) decreases, as the concentration of uric acid is increased.

From Fig. 4 (b), it can be ascertained that the prepared smartphone assisted FO-LRSPR biosensor has linear response towards the uric acid concentration range of 0.01–0.7 mM. Here standard deviation estimated for both the red and blue color channels came out to be about 5%, when the measurements were repeated 5 times. The sensor has high sensitivity values of 1.02/mM and 0.90/mM for blue and red channels respectively, as estimated from their respective slopes. The limit of detection for the fabricated smartphone based FO-LRSPR biosensor came out to be about 0.02 mM.

3.6. Selectivity and interference studies

For the assessment of selectivity of the fabricated smartphone based FO-LRSPR biosensor, various common interferents present in the body like glucose, urea and ascorbic acid of 1 mM concentration were made to interact with the uricase enzyme immobilized on the proposed sensor structure Au/SiO_2/optical-fiber separately and the corresponding values for the blue and red color channel were noted and are shown in Fig. 5 (a). It can be seen from Fig. 5 (a) that the prepared analyte/uricase/Au/SiO_2/optical-fiber sensor structure is extremely selective towards uric acid since no substantial shift in the blue and red color intensity from the reference buffer value is observed for different analytes of 1 mM concentration (Ascorbic acid, Glucose and Urea) in comparison to what was observed for uric acid of 1 mM concentration.

Now, to study the effect of interference of different analytes on the sensing capability of the fabricated smartphone based FO-LRSPR uric acid, 1 mM concentration of Ascorbic acid, Glucose and Urea are spiked with 1 mM concentration of uric acid separately and the respective blue and red color intensities were noted. It can be deciphered from Fig. 5 (b) that the fabricated sensor is very much selective towards uric acid and shows no appreciable shift in the color intensity when uric acid of 1 mM concentration is spiked with interfering analytes of the same concentration. This proves that the fabricated smartphone based FO-LRSPR uric acid biosensor is immune to interference from other analytes.

3.7. Shelf life study

To determine shelf life of the fabricated smartphone based FO-LRSPR biosensor, the response of the sensor was recorded for 0.4 mM concentration of uric acid over a period of 24 weeks at fixed time intervals (every 3 weeks) and is shown in Fig. 5(c). It was determined that the prepared FO-LRSPR sensor retains its 90% activity for 24 weeks and hence it is stable for a minimum period of 24 weeks (Fig. 5(c)).

3.8. Validation of smartphone assisted FO-LRSPR uric acid biosensor

The proposed smartphone assisted FO-LRSPR uric acid biosensor is validated using real serum and urine samples. The fabricated cleaved-clad sensing portion (uricase/Au/SiO_2/optical fiber) is held in contact with the known concentration of uric acid present in real serum and urine samples. 5 different concentrations of uric acid present in human serum sample were held in contact with the sensing portion one by one and the normalized blue color intensity is determined corresponding to different concentrations of uric acid are shown in Supplementary Table S3. The obtained values of blue color intensity were compared to the corresponding values in the calibration curve (Fig. 4 (b)) and the comparison is presented in Supplementary Table S3. Similarly, 5 different concentrations of uric acid present in human urine sample were analyzed and corresponding results are tabulated in Supplementary Table S4. The normalized blue color intensity for all measured concentrations of uric acid in real serum and urine samples is found to be in close proximity to the expected values based on the calibration curve i.e. within 5% acceptable error. Hence, it can be gathered that the proposed smartphone assisted FO-LRSPR biosensor possesses the ability to detect uric acid even in complex and clinically significant urine and serum samples.

3.9. Comparison with reported work

There are several of reports available on electrochemical uric acid biosensors in literature (Zhaoet al., 2013), (Ibupotoet al., 2018). However, these sensors suffer from certain drawbacks such as drying out of electrolyte due to varying conditions of ambient like high temperature

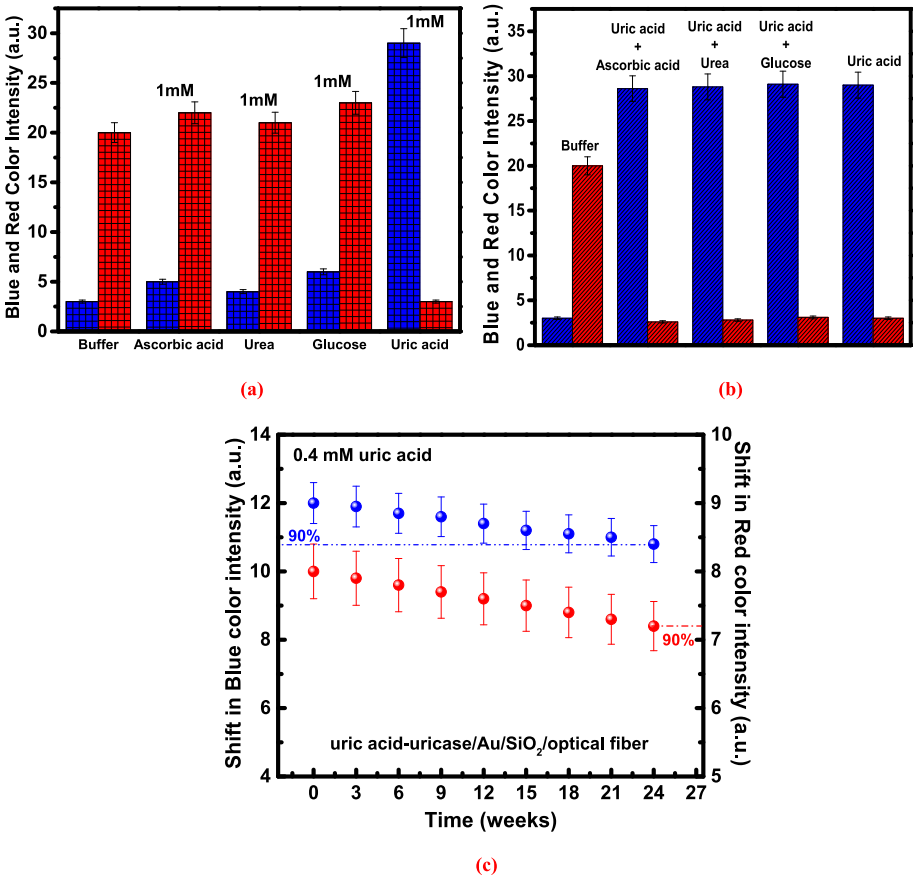

Fig. 5. (a) Selectivity, (b) Interference, and (c) Shelf life, studies performed on the fabricated smartphone assisted FO-LRSPR biosensor.

and low humidity, which in turn decrease the sensor's life and downgrade its stability. Also, due to the requirement of non-biocompatible electron mediating species, they possess environmental damage. It is also often observed that electrochemical biosensors suffer from poor performance and non-specific binding when tested with real complex samples (Putzbach and Ronkainen, 2013). Optical biosensors are better alternative as they have higher sensitivity and higher signal to noise ratio owing to them being resistant to electromagnetic interference. Amongst the various kind of optical biosensors available, SPR based sensors are highly explored due to their higher precision and sensitivity (Wijayaet al., 2011), (Arghir et al., 2015). LRSPR being the advanced version of SPR having better sensitivity is exploited in the recent times for application in biosensors. There are a couple of reports available in literature in which smartphone is integrated with SPR technique for the fabrication of biosensors detecting various analytes. Zhang et al. reported grating coupled SPR technique for the detection of lipopolysaccharides using Au gratings as the sensing element (Zhanget al., 2018). However, the formation of gratings requires difficult process handling and the functionalization of peptides on top of it is a tedious and time consuming task. Au and Ag nanoparticles have been utilized by several research groups in the fabrication of dark field microscopy based SPR sensor, fiber optic localized SPR sensor, colorimetric localized SPR sensor, for various theoretical and experimental studies (Kim et al., 2014)– (Dutta et al., 2016a). However, these sensors lack in terms of experimental detection of biomolecules, bulky setup, no specific studies performed for selectivity and shelf life etc. Au/Ag bilayer was used as sensing matrix in the development of dual FO-SPR, FO-SPR and SPR imaging platform by Liu et al., Liu et al., and Guner et al., respectively (Liu et al., 2018b)– (Guneret al., 2017). These sensors suffer from disadvantages such as no shelf life or selectivity studies. Gold is coupled with Cytop grating substrate to develop SPR sensor working in transmission mode by Lertvachirapaiboon et al. (2018). Cytop being a polymer has certain disadvantages like it does not work at elevated temperatures, posses poor stability etc. Olefin polymer integrated with capped nanoslit array is utilized by Lee et al. for the fabrication of SPR imaging sensor to detect Imidacloprid pesticides (Leeet al., 2016). The technique utilized for the fabrication of this biochip is hot embossing nanoimprint lithography which requires high end equipment and consists of a very tedious process. Table 1 depicts the comparison of such sensors with the smartphone integrated FO-LRSPR biosensor fabricated in the present work. The prepared smartphone integrated FO-LRSPR biosensor effectively overcomes the shortcomings seen in the reported smartphone based SPR sensors (Table 1). To the best of our knowledge, no report on smartphone integrated FO-LRSPR biosensor is reported in literature. The fabricated FO-LRSPR biosensor integrated with smartphone is economical, ability to be used in remote locations, hand-held, possess high sensitivity, selectivity and shelf life. Contrary to the most exploited sensing layers for smartphone based SPR sensors, the dielectric sensing layer SiO_2 used in the present FO-LRSPR smartphone sensor has an easy fabrication process, chemically stable, ecological and economical. The developed smartphone integrated FO-LRSPR biosensor has the potential to overcome the shortcomings such as low precision, low sensitivity etc., faced by the conventional smartphone based SPR sensors.

4. Conclusion

A novel hand-held smartphone assisted FO-LRSPR based biosensor has been developed in the present work and utilized for the uric acid detection in the 0.1 mM to 1 mM concentration range. SiO_2 nanostructured film with tunable refractive index is utilized as the dielectric sensing layer, replacing the most explored Teflon or Cytop. Avantes

Table 1
Assessment of the prepared smartphone assisted FO-LRSPR biosensor as compared to the reported smartphone based SPR biosensors.

Technique	Sensing material/matrix	Sensed element	Performance Characteristics	Reference
Grating-coupled SPR	Au grating and a flat Au film	Lipopolysaccharides	LOD = 32.5 ng/mL in water	Zhanget al. (2018)
Dark field microscopy based SPR	Gold Nanoparticles	Biotin-streptavidin	No performance characteristics evaluated	Kim et al. (2014)
Dual color FO-SPR	Au/Ag Bilayer	Immunoglobulin (IgG)	Resolution = 2.3×10^{-4} RIU No performance characteristics evaluated	Liu et al. (2018b)
Fiber optic localized SPR	Au Nanoparticles	Refractive index sensing	Senstivity = 5.47/RIU Resolution = 3.8×10^{-5} RIU	Liu et al. (2018a)
Colorimetric detection based on localized SPR	Ag Nanoparticles	Ammonia	LOD = 200 mgL^{-1}, Response time = 20 s	Amirjani and Fatmehsari (2018)
Colorimetric Localized surface plasmon resonance	Au Nanoparticles	BSA protein and trypsin enzyme	LOD = 0.28 μm and 1.10 μm Response sensitivity = 17.466 and 12.063	Dutta et al. (2016b)
FO-SPR RGB	Ag/Au bilayer	Refractive index sensing	Sensitivity = 18.59/RIU, Resolution = 5.3×10^{-4} RIU	Liu et al. (2018c)
Surface plasmon resonance imaging (SPRi)platform	Ag/Au bilayer coated Blu-ray disk	IgG	LOD = 4.12×10^{-5} RIU	Guneret al. (2017)
Capped nanoslit based SPR biochip integrated with imaging system	Capped nanoslit array on a cyclic olefin polymer	Imidacloprid pesticides	LOD = 0.2 ng/mL	Leeet al. (2016)
Transmission SPR	Au/CYTOP grating substrate	Refractive index sensing	Sensitivity = 282/RIU	Lertvachirapaiboon et al. (2018)
FO-SPR	Ag	Refractive index sensing	Sensitivity = 5.96×10^{-4} RIU/pixel	Bremer and Roth (2015)
FO-SPR	Au/Cr	Temperature sensor	Sensitivity = −0.0018 a.u./°C	Luet al. (2019)
Transmission SPR	Capped gold nanoslit arrays	Bovin serum albumin (BSA)	LOD = 2.43 μg mL^{-1}	Pan et al. (2018)
Angle-resolved SPR based on a single disposable device	Au/Glass/PDMS	$\beta_2$microglobulin	LOD = 0.1 μg mL^{-1}	Preechaburana et al. (2012)
FO-SPR	Au	Staphylococcal Protein A (SPA) and bovine immunoglobulin G (IgG)	LOD = 47.4 nM	Liu et al. (2015)
FO-LRSPR	SiO_2	Uric acid	Sensitivity = 1.02/mM, LOD = 0.02 mM	Present work

spectrometer is utilized for the spectral measurements of the fabricated FO-LRSPR biosensor. Digital camera of a smartphone has the ability to differentiate between the intensities of different colors. This property is utilized in the present case for the quantification of blue and red color intensities from the LRSPR signal in real time using an android application software, which makes the sensing system immune to any false detection and enhances its sensitivity. The fabricated smartphone assisted FO-LRSPR biosensor is found to have a linear response for the 0.1 mM–0.7 mM concentration range of uric acid, along with a sensitivity of 1.02/mM and LOD of 0.02 mM. The prepared biosensor is found to be selective in nature and its shelf life/stability is assessed to be around 24 weeks. The achieved results prove that the fabricated smartphone assisted FO-LRSPR biosensor is capable of precisely and efficiently detecting uric acid in a broad range of concentration. The proposed FO-LRSPR sensor can be very well employed in the field of point-of-care detection at remote locations where conventional SPR sensors seize to perform well.

CRediT authorship contribution statement

Surbhi Jain: Conceptualization, Methodology, Writing – original draft. **Ayushi Paliwal:** Writing – review & editing, Visualization. **Vinay Gupta:** Review and editing, Conceptualization, Supervision, Resources. **Monika Tomar:** Writing – review & editing, Review and editing, Conceptualization, Supervision, Resources.

Declaration of competing interest

The authors declare that they have no known competing financial interests or personal relationships that could have appeared to influence the work reported in this paper.

Acknowledgment

The authors are grateful to DST, India and University of Delhi for the financial support and the experimental facilities. One of the authors, SJ is grateful to University Grants Commission (UGC), India, for the research fellowship.

Appendix A. Supplementary data

Supplementary data to this article can be found online at https://doi.org/10.1016/j.bios.2021.113919.

References

Amirjani, A., Fatmehsari, D.H., 2018. Colorimetric detection of ammonia using smartphones based on localized surface plasmon resonance of silver nanoparticles. Talanta 176, 242–246.
Arghir, I., Spasic, D., Verlinden, B.E., Delport, F., Lammertyn, J., 2015. Improved surface plasmon resonance biosensing using silanized optical fibers. Sensor. Actuator. B Chem. 216, 518–526.
Arora, S., Kaur, T., Kaur, A., Singh, A.P., 2014. Glycine aggravates ischemia reperfusion-induced acute kidney injury through N-methyl-D-aspartate receptor activation in rats. Mol. Cell. Biochem. 393 (1–2), 123–131.
Batumalay, M., Harun, S.W., Ahmad, F., Nor, R.M., Zulkepely, N.R., Ahmad, H., 2014a. Tapered plastic optical fiber coated with Graphene for uric acid detection. IEEE Sensor. J. 14 (5), 1704–1709. May.
Batumalay, M., Ahmad, F., Lokman, A., Jasim, A.A., Wadi Harun, S., Ahmad, H., 2014b. Tapered plastic optical fiber coated with single wall carbon nanotubes polyethylene oxide composite for measurement of uric acid concentration. Sens. Rev. 34 (1), 75–79. Jan.
Berini, P., 2009. Long-range surface plasmon polaritons. Adv. Opt Photon 1 (3), 484.
Bremer, K., Roth, B., 2015. Fibre optic surface plasmon resonance sensor system designed for smartphones. Opt Express 23 (13), 17179.
Burgess, H.J., Eastman, C.I., 2006. A late wake time phase delays the human dim light melatonin rhythm. Neurosci. Lett. 395 (3), 191–195. Mar.
Dewan, S., Paliwal, A., Tomar, M., Kapoor, A.K., Tandon, R.P., Gupta, V., 2018. Surface plasmon resonance aided analysis of quantum wells for photonic device applications. Mater. Des. 150, 94–103. Jul.
Dutta, S., Saikia, K., Nath, P., 2016a. Smartphone based LSPR sensing platform for bio-conjugation detection and quantification. RSC Adv. 6 (26), 21871–21880.
Dutta, S., Saikia, K., Nath, P., 2016b. Smartphone based LSPR sensing platform for bio-conjugation detection and quantification. RSC Adv. 6 (26), 21871–21880.
Göçenoğlu Sarıkaya, A., Osman, B., Çam, T., Denizli, A., 2017. Molecularly imprinted surface plasmon resonance (SPR) sensor for uric acid determination. Sensor. Actuator. B Chem. 251, 763–772. Nov.

Guner, H., et al., 2017. A smartphone based surface plasmon resonance imaging (SPRi) platform for on-site biodetection. Sensor. Actuator. B Chem. 239, 571–577.
Gupta, B.D., Verma, R.K., 2009. Surface plasmon resonance-based fiber optic sensors: principle, probe designs, and some applications. J. Sensors 2009, 1–12. Aug.
Ibupoto, Z.H., et al., 2018. Synthesis of heart/dumbbell-like CuO functional nanostructures for the development of uric acid biosensor. Materials 11 (8), 1–13.
Jain, S., Paliwal, A., Gupta, V., Tomar, M., 2020a. Refractive index tuning of SiO2 for long range surface plasmon resonance based biosensor. Biosens. Bioelectron. 168, 112508. Nov.
Jain, S., Paliwal, A., Gupta, V., Tomar, M., 2020b. Refractive index tuning of SiO2 for long range surface plasmon resonance based biosensor. Biosens. Bioelectron. 168 (April).
Jindal, K., Tomar, M., Gupta, V., 2017. A novel low-powered uric acid biosensor based on arrayed p-n junction heterostructures of ZnO thin film and CuO microclusters. Sensor. Actuator. B Chem. 253, 566–575. Dec.
Kant, R., Tabassum, R., Gupta, B.D., 2016a. Fiber optic SPR-based uric acid biosensor using uricase entrapped polyacrylamide gel. IEEE Photon. Technol. Lett. 28 (19), 2050–2053. Oct.
Kant, R., Tabassum, R., Gupta, B.D., 2016b. Fiber optic SPR-based uric acid biosensor using uricase entrapped polyacrylamide gel. IEEE Photon. Technol. Lett. 28 (19), 2050–2053.
Kim, B.N., Diaz, J.A., Hong, S.G., Lee, S.H., Lee, L.P., 2014. Dark-field smartphone microscope with nanoscale resolution for molecular diagnostics. 18th Int. Conf. Miniaturized Syst. Chem. Life Sci. MicroTAS 2247–2249, 2014.
Lee, K.L., et al., 2016. Nanoplasmonic biochips for rapid label-free detection of imidacloprid pesticides with a smartphone. Biosens. Bioelectron. 75, 88–95.
Lertvachirapaiboon, C., Pothipor, C., Baba, A., Shinbo, K., Kato, K., 2018. Transmission surface plasmon resonance image detection by a smartphone camera. MRS Commun. 8 (3), 1279–1284.
Liu, Y., Liu, Q., Chen, S., Cheng, F., Wang, H., Peng, W., 2015. Surface plasmon resonance biosensor based on smart phone platforms. Sci. Rep. 5, 1–9.
Liu, Q., Liu, Y., Yuan, H., Wang, J., Guang, J., Peng, W., 2018a. Smartphone based LSPR biosensor. Asia Commun. Photonics Conf. ACP 2018. Octob, pp. 2018–2020.
Liu, Q., Yuan, H., Liu, Y., Wang, J., 2018b. Real-time biodetection using a smartphone-based dual-color surface plasmon resonance sensor. J. Biomed. Opt. 23, 1, 04.
Liu, Q., Liu, Y., Yuan, H., Wang, F., Peng, W., 2018c. A smartphone-based red-green dual color fiber optic surface plasmon resonance sensor. IEEE Photon. Technol. Lett. 30 (10), 927–930.
Lu, X., et al., 2012. Detection of ractopamine residues in pork by surface plasmon resonance-based biosensor inhibition immunoassay. Food Chem. 130 (4), 1061–1065. Feb.
Lu, L., et al., 2019. A portable optical fiber SPR temperature sensor based on a smartphone. Opt Express 27 (18), 25420.
Méjard, R., Griesser, H.J., Thierry, B., 2014. Optical biosensing for label-free cellular studies. TrAC Trends Anal. Chem. (Reference Ed.) 53, 178–186.
Mudanyali, O., Dimitrov, S., Sikora, U., Padmanabhan, S., Navruz, I., Ozcan, A., 2012. Integrated rapid-diagnostic-test reader platform on a cellphone. Lab Chip 12 (15), 2678–2686. Aug.
Paliwal, A., Tomar, M., Gupta, V., 2018. Refractive index sensor using long-range surface plasmon resonance with prism coupler. Plasmonics 1–7. Jul.
Pan, M.Y., Lee, K.L., Lo, S.C., Wei, P.K., 2018. Resonant position tracking method for smartphone-based surface plasmon sensor. Anal. Chim. Acta 1032, 99–106.
R. A. Potyrailo et al., "Wireless sensors and sensor networks for homeland security applications," Trac. Trends Anal. Chem., vol. 40. Elsevier, pp. 133–145, 01-Nov-2012.
Preechaburana, P., Gonzalez, M.C., Suska, A., Filippini, D., 2012. Surface plasmon resonance chemical sensing on cell phones. Angew. Chem. Int. Ed. 51 (46), 11585–11588.
Putzbach, W., Ronkainen, N., 2013. Immobilization techniques in the fabrication of nanomaterial-based electrochemical biosensors: a review. Sensors 13 (4), 4811–4840. Apr.
Rakow, N.A., Suslick, K.S., 2000. A colorimetric sensor array for odour visualization. Nature 406 (6797), 710–713. Aug.
Ringertz, H., 1965. Optical and crystallographic data of uric acid and its dihydrate. Acta Crystallogr. 19 (2), 286–287. Aug.
A. Roda, E. Michelini, M. Zangheri, M. Di Fusco, D. Calabria, and P. Simoni, "Smartphone-based biosensors: a critical review and perspectives," Trac. Trends Anal. Chem., vol. 79. Elsevier B.V., pp. 317–325, 01-May-2016.
Srivastava, S.K., Verma, R., Gupta, B.D., 2011. Surface plasmon resonance based fiber optic sensor for the detection of low water content in ethanol. Sensor. Actuator. B Chem. 153 (1), 194–198.
Tseng, D., et al., 2010. Lensfree microscopy on a cellphone. Lab Chip 10 (14), 1787–1792. Jun.
Wark, A.W., Lee, H.J., Corn, R.M., 2005. Long-range surface plasmon resonance imaging for bioaffinity sensors. Anal. Chem. 77 (13), 3904–3907.
Wijaya, E., et al., 2011. Surface plasmon resonance-based biosensors: from the development of different SPR structures to novel surface functionalization strategies. Curr. Opin. Solid State Mater. Sci. 15 (5), 208–224. Oct.
Zangheri, M., et al., 2015. A simple and compact smartphone accessory for quantitative chemiluminescence-based lateral flow immunoassay for salivary cortisol detection. Biosens. Bioelectron. 64, 63–68. Feb.
Zhang, J., et al., 2018. Lipopolysaccharides detection on a grating-coupled surface plasmon resonance smartphone biosensor. Biosens. Bioelectron. 99, 312–317. July 2017.
Zhao, Y., et al., 2013. Highly sensitive uric acid biosensor based on individual zinc oxide micro/nanowires. Microchim. Acta 180 (9–10), 759–766. Jul.
's-Gravenmade, E.J., Vogels, G.D., van Pelt, C., 2010. Preparation, properties and absolute configuration of (-)-allantoin. Recl. des Trav. Chim. des Pays-Bas 88 (8), 929–939. Sep.